Journal of Hydrology 560 (2018) 546–559

Contents lists available at ScienceDirect

Journal of Hydrology

journal homepage: www.elsevier.com/locate/jhydrol

Research papers

Sensitivity of peak flow to the change of rainfall temporal pattern due to warmer climate

Sherien Fadhel [a,b,*], Miguel Angel Rico-Ramirez [a], Dawei Han [a]

[a] Department of Civil Engineering, University of Bristol, Bristol, United Kingdom
[b] Department of Water Resources Engineering, University of Al-Mustansiriyah, Baghdad, Iraq

ARTICLE INFO

Article history:
Received 13 April 2017
Received in revised form 28 February 2018
Accepted 16 March 2018
Available online 17 March 2018
This manuscript was handled by A. Bardossy, Editor-in-Chief, with the assistance of Uwe Haberlandt, Associate Editor

Keywords:
Rainfall temporal pattern
Scaling for rainfall volume and fraction
Climate change
Peak flow

ABSTRACT

The widely used design storms in urban drainage networks has different drawbacks. One of them is that the shape of the rainfall temporal pattern is fixed regardless of climate change. However, previous studies have shown that the temporal pattern may scale with temperature due to climate change, which consequently affects peak flow. Thus, in addition to the scaling of the rainfall volume, the scaling relationship for the rainfall temporal pattern with temperature needs to be investigated by deriving the scaling values for each fraction within storm events, which is lacking in many parts of the world including the UK. Therefore, this study analysed rainfall data from 28 gauges close to the study area with a 15-min resolution as well as the daily temperature data. It was found that, at warmer temperatures, the rainfall temporal pattern becomes less uniform, with more intensive peak rainfall during higher intensive times and weaker rainfall during less intensive times. This is the case for storms with and without seasonal separations. In addition, the scaling values for both the rainfall volume and the rainfall fractions (i.e. each segment of rainfall temporal pattern) for the summer season were found to be higher than the corresponding results for the winter season. Applying the derived scaling values for the temporal pattern of the summer season in a hydrodynamic sewer network model produced high percentage change of peak flow between the current and future climate. This study on the scaling of rainfall fractions is the first in the UK, and its findings are of importance to modellers and designers of sewer systems because it can provide more robust scenarios for flooding mitigation in urban areas.

1. Introduction

The accurate design of urban drainage networks requires the continuous simulation of long rainfall time series using an urban drainage model, which results in long computational times, and later the results need to be statistically post-processed (Willems 2013; Butler and Davies 2011). To overcome this problem, a design rainfall hyetograph with a specific temporal pattern, which is known as a design storm, is used instead in practice (Yen and Chow 1980; Wenzel 1982; Willems 2000; Madsen et al. 2002). Design storms can be derived by following one of two distinct approaches. The first approach is to extract the rainfall intensity from intensity–duration–frequency (IDF) curves and apply an arbitrary temporal distribution to that intensity to obtain the design storm (Kiefer and Chu, 1957; Desbordes, 1978). The second approach is to analyse specific storm events from the observed rainfall data to derive the temporal distribution (Huff, 1967; Nguyen et al., 2010). For both approaches a statistical analysis is performed before the hydrological model simulations. The statistical analysis has assumed that the frequency of urban drainage peak flow is equal to the corresponding frequency of the rainfall event. Such assumption is applied for areas that have a large proportion of paving, which is most often the case for urban runoff. Also, when the concentration time is almost constant for a specific location in the drainage system. In addition, such areas should have no strong seasonal variation such as watershed hydrology where the soil saturation level can affect the runoff. For the above conditions, the high rainfall intensities at a given location result in large peak sewer flows.

Different design storms have been derived, developed, and adopted around the world. Kiefer and Chu (1957) were the first to develop the Chicago storm in the USA, and later other alternative patterns were developed; for example, by Sifalda (1973), Pilgrim and Cordery (1975), the UK *Flood Studies Report* (FSR, 1975), Desbordes (1978), Yen and Chow (1980), and the UK *Flood Estimation Handbook* FEH (1999). The drawbacks of these

* Corresponding author at: Department of Water Resources Engineering, University of Al-Mustansiriyah, Baghdad, Iraq.
E-mail address: sa12372@my.bristol.ac.uk (S. Fadhel).

https://doi.org/10.1016/j.jhydrol.2018.03.041
0022-1694/© 2018 Elsevier B.V. All rights reserved.

approaches have been summarised in many previous studies (McPherson, 1978; Walesh, 1979; James and Robinson, 1982; Rivard, 1996). One of the shortcomings of these approaches that this study seeks to address concerns the fixing of the shape of the temporal pattern for rainfall storms regardless of changes in the climate. Using the current approaches, a specific current rainfall intensity is expected to appear in the future but with a shorter return period (IPCC, 2012). If we apply the temporal pattern of any of the abovementioned design storms for this rainfall intensity and for two different climates (i.e. current and future climates), the two storms will end up with exactly the same temporal distribution and peaks at the same location. However, Wasko and Sharma (2015) showed that the rainfall temporal pattern in Australia is changing with temperature due to climate change. The observed relation between rainfall and temperature, which is known as scaling, results from the natural variability in the present climate. The authors investigated the scaling values for each fraction of the rainfall temporal pattern and have found that the highest rainfall fraction scales positively, while the lowest fraction scales negatively with temperature regardless of the season and the type of event (see Fig. 1 in Wasko and Sharma 2015). The adjustment of the temporal pattern for a range of temperature changes using different scaling values for different locations (depending on the location of the station where the scaling is derived) was found to greatly affect the peak flood value in these locations (Wasko and Sharma, 2015). Another recent study by Müller et al. (2017) confirms the findings of Wasko and Sharma, 2015 in which changing the shape of rainfall event has a great effect on the peak flow of combined sewer system. However, the authors in Müller et al. (2017) study adopt a continuous rainfall time series instead of design storms.

For the UK climate, all the previous studies have investigated the scaling relationship concentrated on the scaling of the overall storm event intensity, termed as storm volume, and the most recent of these studies have investigated such a relation for sub-daily data, and more specifically for extreme hourly data (Jones et al., 2014; Blenkinsop et al., 2015; Chan et al., 2016). However, none of the previous studies examined the scaling values for the UK climate for the individual fractions of storm event (i.e. rainfall temporal pattern) (see Section 3.1 for the definitions and more details of rainfall volume and rainfall fractions). It would be of interest to the hydrological community to explore such an issue besides Australia so that a more complete pattern around the world could be derived.

Thus, the objectives of this study are to: (1) study the scaling relationship for both the storm volume and the individual fractions of the storm event, termed the temporal pattern; for storms with and without seasonal separation and (2) investigate how a change in the temporal pattern can affect the peak flow of the sewer system of a particular urban area for the future climate.

2. Catchment and observed data

The study area, which is a small urban catchment with an area of approximately 12 km $\times$ 5 km, is located in West Yorkshire in the north of England. The UK Environment Agency (EA) provides rainfall data at a 15-min temporal resolution from tipping bucket gauges that cover large parts of the UK. However, all the gauges provided by the EA were located outside the study area, thus only the 28 closest gauges were used for this study (Fig. 1). As shown in Fig. 1, some of the gauges are located far away from the catchment at distances of more than 40 km. Thus they may not seem relevant to the study area. However, these gauges were included in order to investigate whether there is a link between scaling values and altitude, as concluded by Wasko and Sharma (2015) for Australia, or not as found by Blenkinsop et al. (2015) for the UK. A quality check of the gauges was performed by using the procedure in Fadhel et al. (2016). The procedure consists of two steps: First, the spatial consistency between nearby gauges is tested (i.e. the gauge being tested is compared with neighbouring gauges). Second, the gauges that are flagged up as a result of the first check are subjected to another test using radar data. This is because rainfall is highly variable in space and time, so the performance of a gauge during a convective storm is not necessarily consistent spatially with that of neighbouring gauges. It should be noted that when the period of rainfall data for the gauges was not covered by the radar data (i.e. before 2006 in this study) only the first quality check was used. The temporal coverage for each gauge is shown in the table in Fig. 1.

The daily temperature data used in this study was the gridded temperature data provided by the climate hydrology and ecology research support system meteorology dataset (CHESS-met) (1961–2015) and was at the 1-km space scale. The CHESS-met air temperature was derived by Robinson et al. (2015) for a reference height of 1.2 m. The authors interpolated the MORECS air temperature from a scale of 40 km to a 1-km resolution based on the bicubic spline method. Later, the integrated hydrological digital terrain model was adopted to adjust the elevation for each pixel of the 1-km grid interpolated data. The 1-km spatial resolution of temperature data may be too high for daily data and lower resolution data could also (or better) be used. Further studies are needed based spatial correlation or semivariograms in order to work out the spatial variability of temperature distribution in the study area. A suitable spatial temperature resolution could then be derived.

The CHESS-met temperature data for the period 2004–2015 was used alongside the rainfall data to derive the scaling values.

3. Methodology

3.1. Scaling for rainfall volume and rainfall temporal pattern

The procedure in Wasko and Sharma (2015) was adopted to study the scaling relationship for both the storm volume (which is defined as the total rainfall depth in mm for a given storm event duration) and the storm fractions for five different durations. The largest 500 storm events in terms of volume for each rain gauge within the common period for all gauges (2004–2015) and a given duration were chosen (Wasko and Sharma, 2015). Extracting such a high number of events ensures that all the heavy rainfall events that occur over the year are considered. Independent events were identified by using the criteria defined in Willems (2000), where two extreme events should be separated by at least a 12-h time interval if the duration is less than 12 h, while for longer durations a time interval larger than the considered duration should be used to delineate the independent events.

Various storm event durations, ranging from 1 h to 24 h, were included in the study (the values of the durations are shown in Fig. 3). Since the gauge network used in this study has a 15-min resolution, the maximum number of fractions for a storm duration of 1 h can only be four (i.e. each fraction has a timescale of 15 min). Thus, to be consistent with storms of other durations the fractions also need to be four in number as well. Therefore, for each duration, the precipitation records were accumulated to ensure that the storm events were grouped in exactly four periods in length. For example, to analyse a 3-h storm event, the rainfall was accumulated into durations of 45 min to end up with a storm of four increments of equal duration. Similarly, a 6-h storm event was split into four increments consisting of four 90-min increments. Later, each storm event was matched to its concurrent temperature.

Most of the previous studies adopt the binning method to derive the scaling values for the rainfall-temperature relationship. The method involves binning rainfall data in temperature bins so

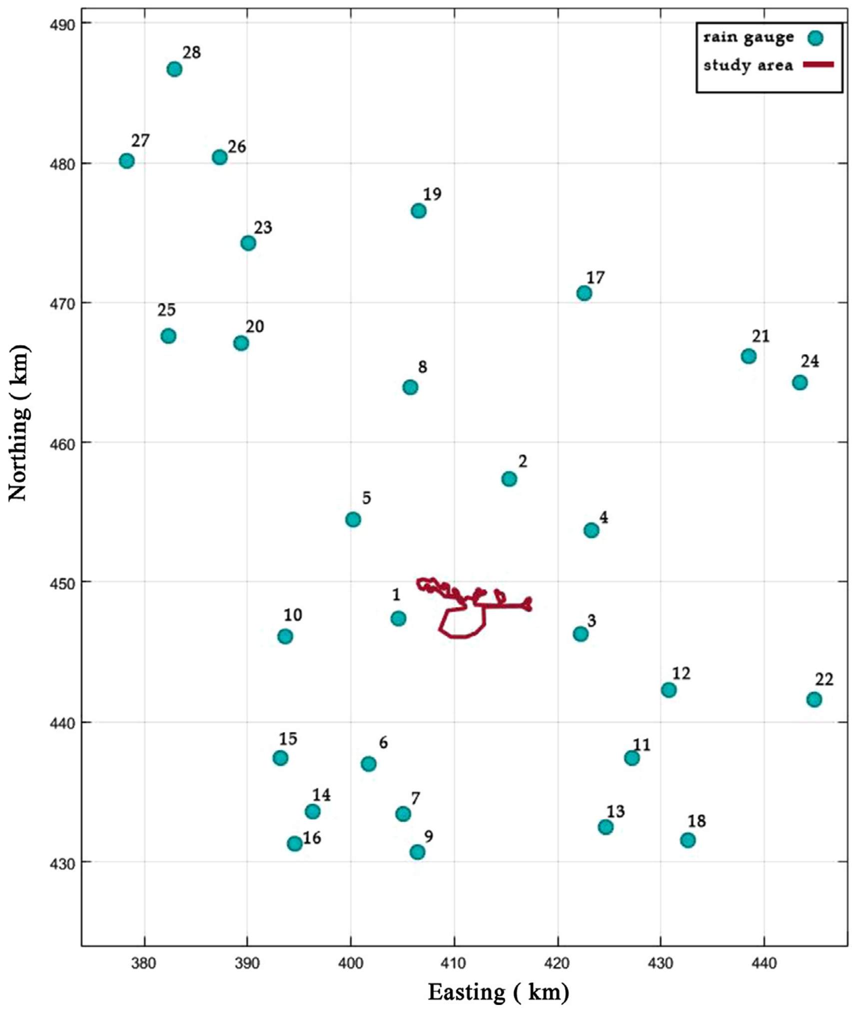

No.	From	To
1	2001	2016
2	2000	2016
3	1985	2015
4	1997	2015
5	1986	2016
6	2000	2016
7	2000	2016
8	2000	2016
9	2002	2016
10	2005	2016
11	1996	2016
12	1986	2016
13	1987	2016
14	2004	2016
15	1998	2016
16	1987	2016
17	1989	2015
18	1986	2016
19	1988	2015
20	1984	2014
21	2004	2015
22	1987	2016
23	2004	2015
24	1985	2015
25	1990	2016
26	2004	2015
27	1994	2016
28	1985	2015

Fig. 1. Study area and location of rain gauges. The number above each gauge (which is based on the distance of the gauge from the centre of the study area) is also used in the table that shows the temporal coverage for each gauge.

that later the trend in the rainfall percentiles in each bin with temperature can be investigated (Lenderink and van Meijgaard, 2008; Hardwick-Jones et al., 2010; Lenderink et al., 2011). However, Wasko and Sharma (2014) showed that the binning method was sensitive to the sample size, whereas quantile regression is unbiased towards the size. The quantile regression derives the scaling of rainfall volume (α_v) with temperature by fitting an exponential regression model to rainfall-temperature pairs, where the logarithm of rainfall volume was regressed against temperature for the high percentile *q99* (Hardwick-Jones et al., 2010; Wasko and Sharma, 2014, 2015). Therefore, in this study, a quantile regression was performed by using the R package, 'quantreq' (Koenker, 2013) to find the scaling values for storms with and without seasonal separation.

To construct the temporal patterns, the storm event was divided by its volume, then each fraction within the pattern was ranked from the largest to the smallest. The scaling of the ranked fractions with temperature was found by fitting the following equation (Wasko and Sharma 2015):

$$P^i_{T+\Delta T} = P^i_T (1+\alpha_i)^{\Delta T} \quad (1)$$

where α_i is the rate at which the rainfall proportion for rank i of the temporal pattern changes per degree of temperature; P^i_T is the ith rank rainfall fraction corresponding to temperature T; and ΔT is the difference in Temperature. The statistical significance of the results at the 95% level was tested by using a t-test for the hypothesis that the slope of the regression line differs from zero against the null hypothesis that the slope is zero. In addition, the confidence intervals (i.e. uncertainty bound) of the scaling results were obtained under the same assumption. These confidence intervals are computed by the rank inversion method (Koenker, 2005).

It is worth noting that the length of the data used in this study was 12 years (i.e. the common period between the gauges), which is consistent with the temporal coverage investigated in previous studies that address the scaling relation (Hardwick-Jones et al., 2010; Wasko and Sharma 2014). However, one could argue that this data length is insufficient and may produce high uncertainty in the scaling results. Therefore, we investigated the effect of the temporal length on the scaling values (see Section 4.2.3.2) to explore how the data length affects the uncertainty of the results.

3.2. Urban runoff model and hydrodynamic sewer flow model

The major parts of the sewer system in the study area carry both the urban rainfall runoff and the domestic and trade wastewater. The modelled sewer system was formed of 444 links, 432 nodes, 13 pumps, and 134 sub-catchments. The areas of sub-catchments ranged in size from 0.1 to 300 ha, and the total length of the sewer conduits was approximately 60 km. The total contributing area of the sub-catchments was 11.06 km^2, where 0.71 km^2 was classed as impermeable and 10.35 km^2 as pervious (Liguori et al. 2012;

Rico-Ramirez et al. 2015). The study area was located in the Pennine Hills, thus the sewer system is relatively steep.

The rainfall-runoff process for the urban area in addition to the flow through the sewer network conduits was modelled by using a hydrodynamic sewer network model (Infoworks CS) in order to study the sensitivity of the peak flow to the change in the rainfall temporal pattern due to warmer climate. A combination of models for rainfall-runoff volume and runoff routing for the different sub-catchments are available in the Infoworks CS model. For example, the New UK Percentage Runoff model (Packman, 1990) is used to find the runoff volume for pervious areas, while the Wallingford model or the fixed runoff coefficient is used for impermeable areas. The catchment runoff routing was found by using the Double Linear Reservoir model (Sarginson and Nussey 1982). The Infoworks CS software calculates the flow through the sewer conduits by solving the full St Venant equations.

The Infoworks CS sewer model was calibrated by following the current UK industrial practice (WaPUG, 2002). The range of rainfall depths and peak rainfall intensities for the three events used for the model calibration were between 9.8 and 35 mm and 6.0 and 14.4 mm/h, respectively (Liguori et al., 2012; Rico-Ramirez et al., 2015). In 2007, seven depth monitors and sixteen flow monitors were installed in the sewer system and upstream of most of the pumping stations (Liguori et al., 2012). These monitors collected data at a frequency of 2 min. The locations of the flow monitors which are shown in the schematic plot of the monitoring network in Fig. 2, were adopted to address the sensitivity of peak flow to the change of rainfall temporal pattern at each location. The main combined sewer overflow structure that serves the centre of the study area is located just downstream of the flow monitors FM015 and FM115 and upstream of FM017. In Section 4.3, the results for flow monitor FM015 are discussed in more detail due to the sensitive location of this flow monitor; however, the results for other 15 flow monitors are also investigated.

4. Results and discussion

4.1. Scaling values for all storms without seasonal separation

The scaling values for storm volumes and fractions were investigated for storms with and without seasonal separation. For the data without seasonal separation, Fig. 3 shows the scaling of five different durations storm event volume (α_v) at each gauge. For hourly storm event volume where a statistically significant positive scaling for storm volume of 1.6% per °C to 4.88% per °C is shown by most of the gauges for the high percentile *q99* (Fig. 3 top left). These results are consistent with Blenkinsop et al. (2015) in which there is no pattern that may refer to regional climatic controls on the scaling relationship between rainfall and temperature (i.e. there is no link between scaling values and altitude).

Subsequently, each hourly storm event was divided into four periods, each having a duration of 15 min. For the largest rainfall fraction (α_1) and the high percentile *q99*, almost all the sites show a statistically significant positive scaling of approximately 0.8–3.3% per °C (Fig. 4). In contrast, all the sites show a negative scaling for the smallest rainfall fraction (α_4) with a magnitude ranging from −0.06% to −1% per °C. However, the results are statistically significant for only a few sites. Also, the number of sites that show statistically significant results for the four fractions is higher for the first fraction, and decreases gradually to the last fraction (Fig. 4). However, the negative scaling for the smallest rainfall fraction within the storm event means that such a fraction is scaling negatively even though the entire storm volume is scaling positively. In addition, the scaling values for the second fraction range between 0.8 and 2% per °C, while only the third fraction gives mixed results (i.e. negatively and positively statistically significant scaling in the range of −0.8% to 0.9% per °C).

An analysis of the results for the four fractions revealed a transition in the scaling values from the largest to the smallest fraction, where the highest positive scaling with temperature is shown by the first rank fraction, while the fourth rank fraction shows the highest negative scaling with temperature. The intermediate fractions exhibit a declining scaling with increasing rank. In Wasko and Sharma (2015), the temporal patterns of most of the sites showed a peak-like structure, where, on average, the greatest magnitude occurs in the second rainfall fraction (see Fig. S4 in Wasko and Sharma, 2015). However, the results of this study reveal that the structure of the temporal pattern varies across the different durations and according to whether the data are seasonally separated or not. For example, structure (A) in Fig. 5 is shown by most of the durations, especially the summer season (discussed in the next

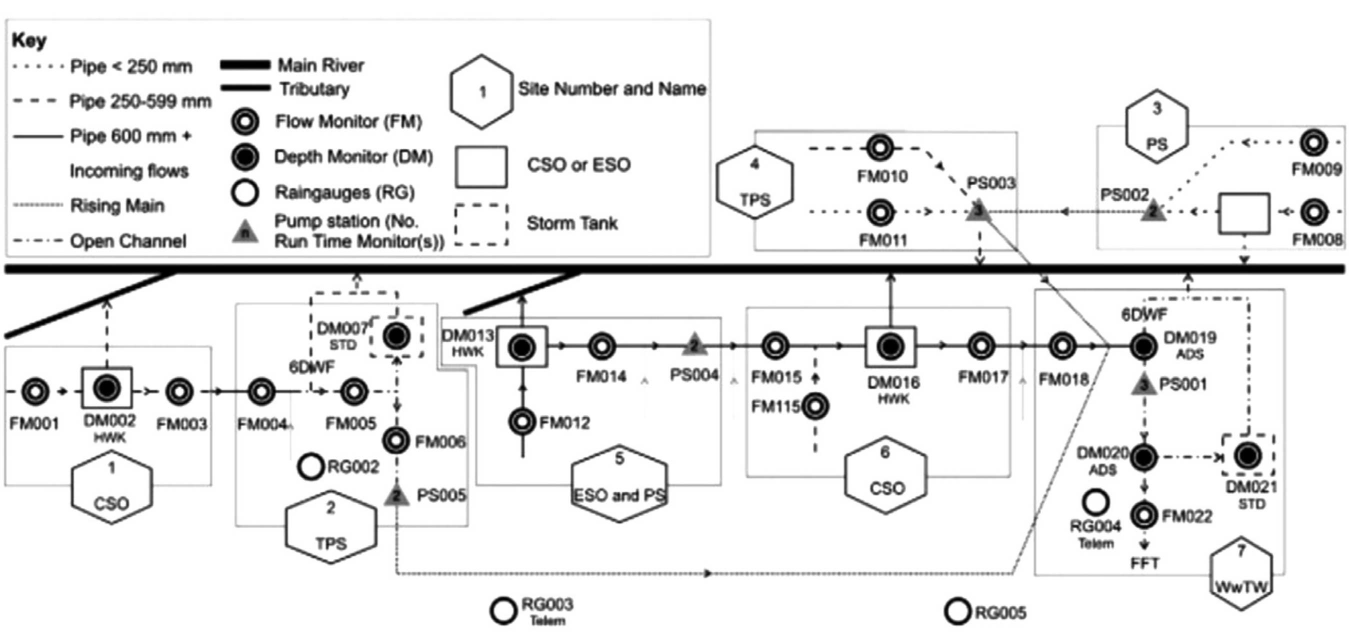

Fig. 2. Schematic overview of the monitoring network (Liguori et al. 2012).

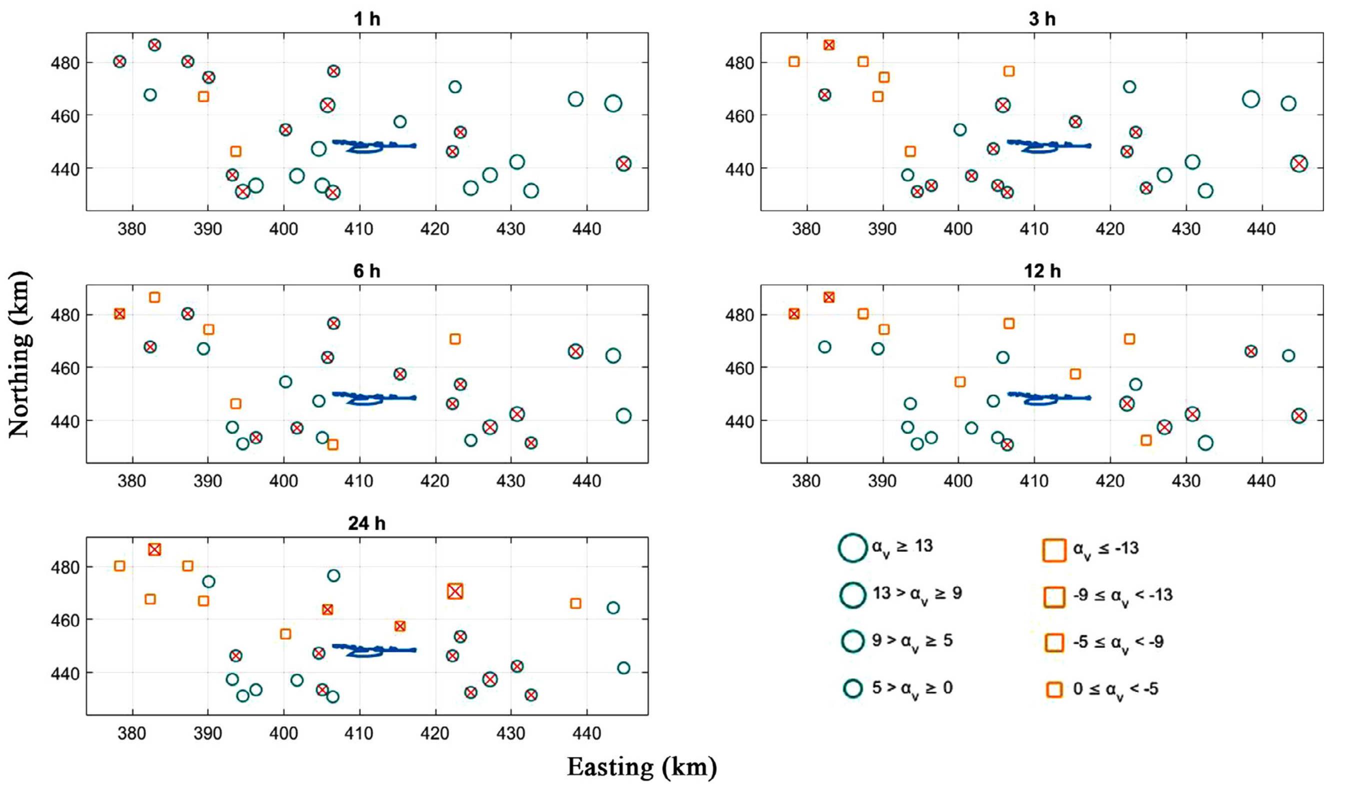

Fig. 3. Rainfall scaling volume for all storms without seasonal separation. Each subplot is for a specific duration. Green circles correspond to positive scaling, while orange squares correspond to negative scaling. Crosses indicate statistical significance at the 95% confidence level. (For interpretation of the references to colour in this figure legend, the reader is referred to the web version of this article.)

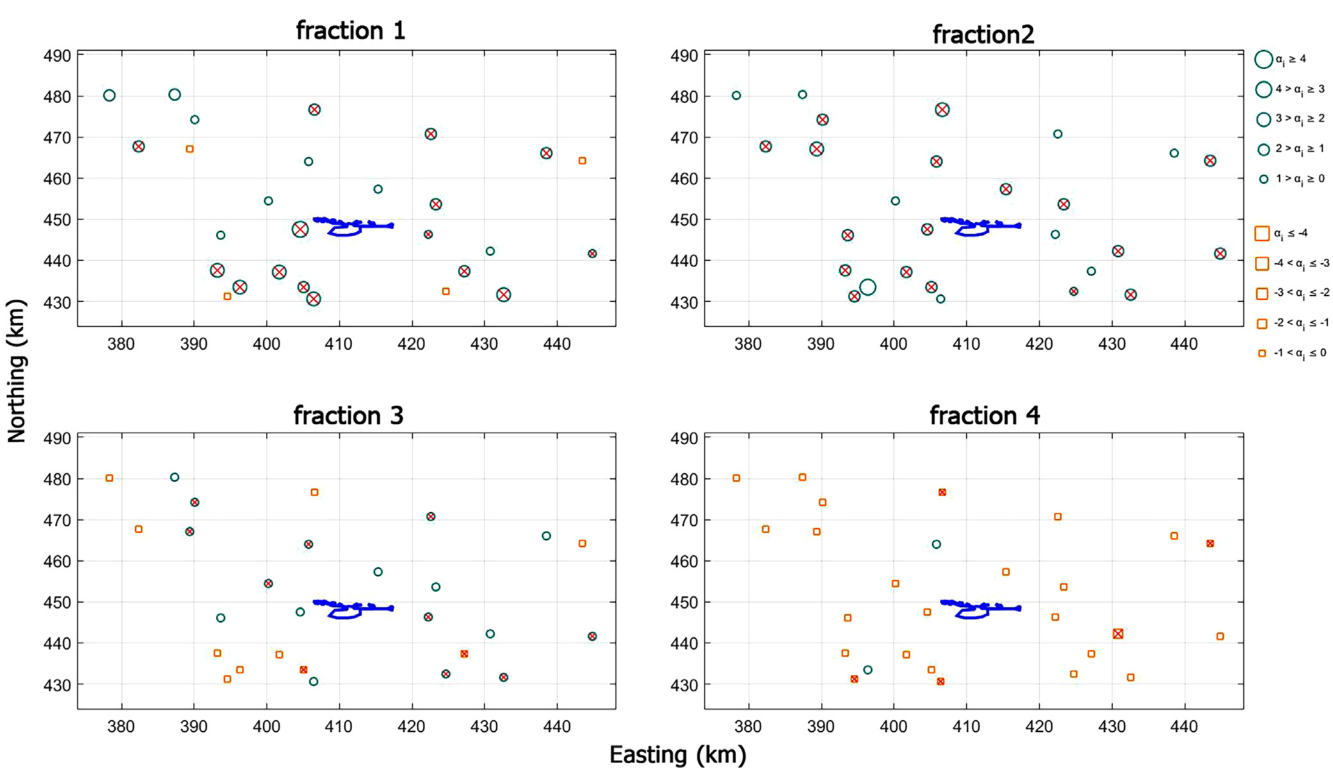

Fig. 4. Scaling for rainfall fractions for hourly storm event (storms without seasonal separation). Green circles correspond to positive scaling, while orange squares correspond to negative scaling. Crosses indicate statistical significance at the 95% confidence level. (For interpretation of the references to colour in this figure legend, the reader is referred to the web version of this article.)

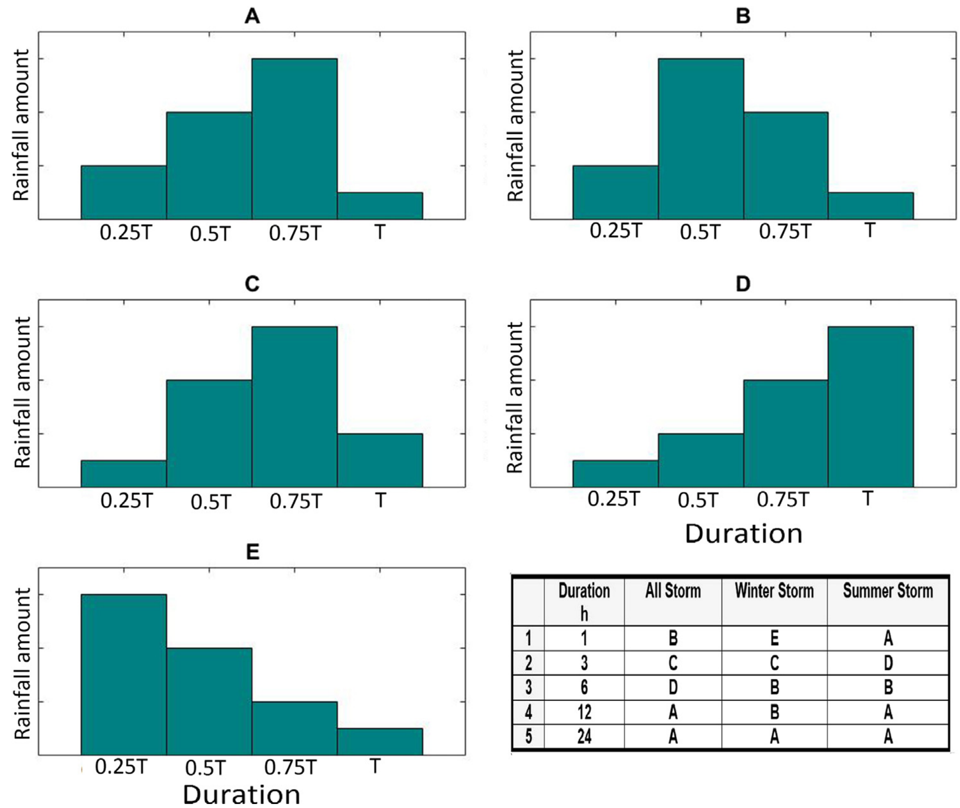

	Duration h	All Storm	Winter Storm	Summer Storm
1	1	B	E	A
2	3	C	C	D
3	6	D	B	B
4	12	A	B	A
5	24	A	A	A

Fig. 5. Derived structure types for the dominant rainfall temporal pattern depending on rainfall duration and weather the data are seasonally separated or not. The index T correspond to the length of rainfall duration.

section). The Table in Fig. 5 shows the structure type of the temporal pattern for each duration, and for storms with and without seasonal separation.

The above analysis of scaling for rainfall volume and fractions was repeated for the other four storm durations, and for each duration considered, the temporal pattern consisted of four equal periods. For almost half of the sites the scaling of the volume decreases further as the storm duration lengthens (Fig. 3). The scaling for the rainfall fractions was found to be consistent for all durations, in that the peak/weaker fraction becomes more/less intense at higher temperatures, regardless the significance of the results over the durations. However, from a comparison of the magnitude of scaling for each segment of the temporal pattern with the corresponding segments for different durations, no obvious trends were observed. It is worth noting that the scaling values for all rainfall fractions and the high percentile *q99* were insignificant for all gauges and the last two durations. While for the second and third durations, the number of the gauges that show significant results were consistent with that of 1 h duration in which it decreasing gradually from the first to the last fraction.

In addition, the range of uncertainty for the scaling results (i.e. both the scaling volume and the rainfall fractions) was checked. For the scaling volume, the uncertainty bound for most of the gauges is within the limit of −1.5 to 5. This is the case for all durations except the first duration (i.e. 1 h), where the uncertainty limit is between −1 and 8 (Fig. 6). However, only a few gauges have an uncertainty range that is higher than the previous limits. Regarding the uncertainty bound for the rainfall fractions, such range shows a transition in the limit values between the fractions, which is consistent with the transition in the scaling values from the largest to the smallest fraction. For example, Fig. 7 shows that the uncertainty range for the first fraction of the hourly storm duration is between −0.8 and 2.5 for most of the gauges. This limit changes gradually from −1 and 2.5 and −1.8 and 0.8 for the second and third fractions, respectively, while the range of uncertainty for the last fraction is between −1.8 and 0.5. Also, the bound of uncertainty for the rainfall fractions is different for different storm durations. However, the uncertainty results for rainfall fractions are consistent to those for the hourly duration, in that the bound of uncertainty changes gradually across rainfall fractions (i.e. from the first fraction to the fourth fraction).

4.2. Scaling values for storms with seasonal separation

Previous studies have shown that the season and the storm type can affect the rainfall-temperature scaling relationship due to the various temperature ranges examined and the nature of the various storm types that are predominant during the different seasons (Berg et al., 2009; Berg et al., 2013; Wasko and Sharma, 2014, 2015). In this study, only a seasonal analysis was performed because Rico-Ramirez et al. (2015) showed that for the same UK study area, most of the convective storms fall within the summer season while stratiform storms occur during the winter season. In addition, the results of an analysis of the peaks over threshold events as well as the median annual maxima statistic reported in Blenkinsop et al. (2015) showed that extreme hourly convective events are most likely to occur in the summer season for most of the locations in the UK. Thus, no separate analysis of storm type is presented in this study.

For the UK, Blenkinsop et al. (2015) showed that the largest scaling value is seen in the summer season (6.9% per °C), while for the other seasons it is lower: 3.2% per °C for winter, 4.7% per °C for spring, and 3.9% per °C for autumn. From a comparison of the results in Blenkinsop et al. (2015) with the above results for

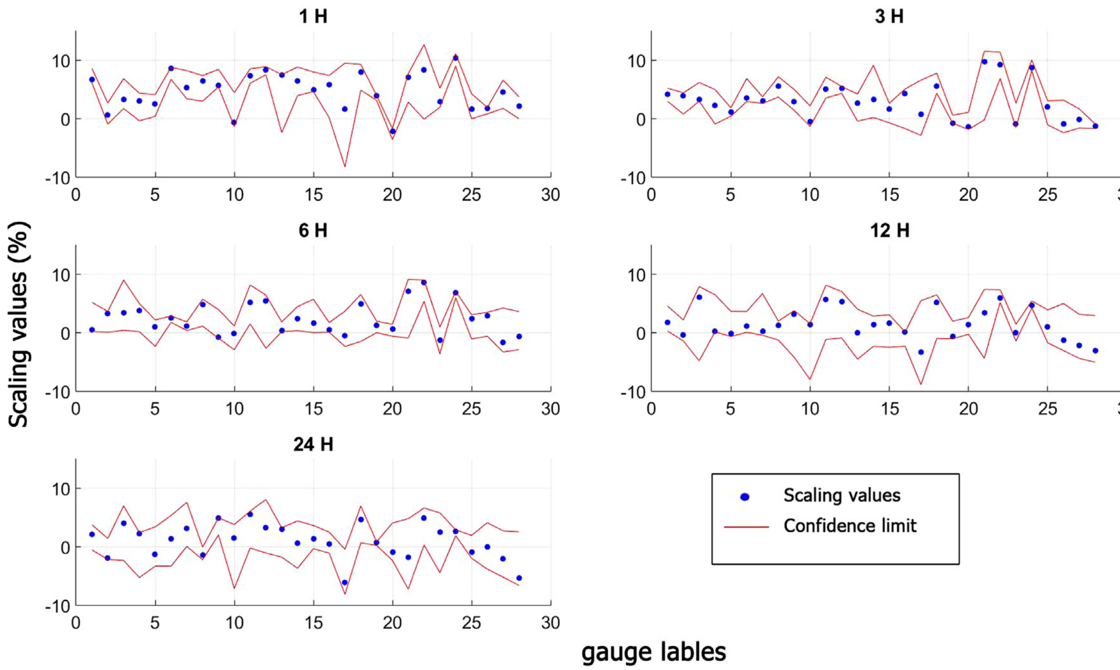

Fig. 6. Uncertainty bounds of the 95% significant level for rainfall scaling volume and all storms without seasonal separation. Each subplot is for a specific duration.

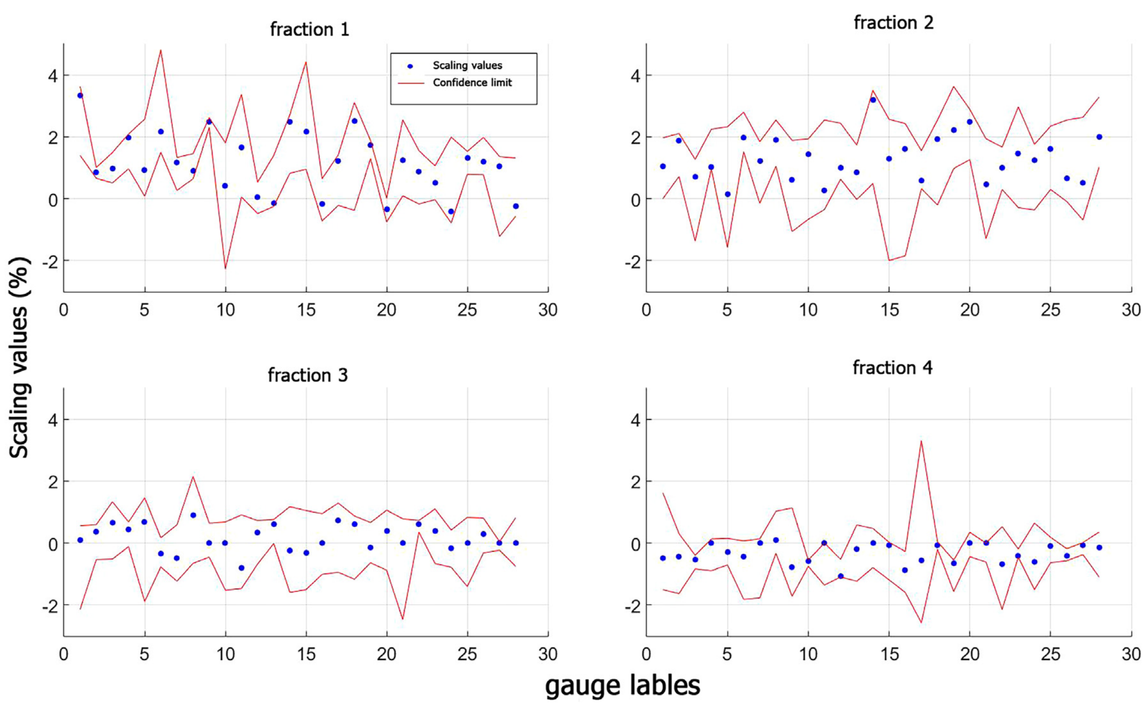

Fig. 7. Uncertainty bounds of the 95% significant level for rainfall fractions and hourly storm events (storms without seasonal separation). Each subplot is for a specific fraction.

the scaling of storms without seasonal separation, it is very clear that seasonal scaling in the UK is considerably different from the scaling value for storms without seasonal separation. In contrast, in Australia, Wasko and Sharma (2015) found that the scaling values for storms with and without seasonal separation were almost the same. This is because in the northern half of Australia summer precipitation is dominant, while winter precipitation is dominant in the southern half of Australia.

4.2.1. Scaling values for summer season storms

In this study, the scaling values for both the storm volume and the fractions were found for the summer (JJA) and winter (DJF) seasons. Fig. S1 in the Supplementary material shows the scaling value for summer rainfall volume and five durations. It is clear from the figure that the scaling value for the high percentile *q99* and hourly summer rainfall is consistent with Blenkinsop et al. (2015), where $\alpha_v \approx 9.2\%$ per °C for the middle of the UK (see Fig. 3 in Blenkinsop

et al., 2015). It is also clear from Fig. S1 that the scaling value for summer rainfall volume falls as the rainfall duration increases. Negative scaling values are shown by only a few stations from the second duration, such a number of stations with negative values increased gradually with duration increase to peak at the 12 h duration. However, some gauges show the opposite result, where the scaling starts to rise once again for the 24-h storm duration. This might have occurred because not all summer storms are convective; some are a mixture of convective and stratiform storms, which affects the signal of scaling (Berg and Haerter, 2011). Another explanation for this might be because of the short sample size which affects the scaling values. Such positive scaling values for 24 h duration must be excluded from the summer storms since it provides false results. However, we have kept it only to show the reader which gauges have untrusted results for a longer duration.

In addition, the scaling values for the 1-h duration and different percentiles (*q99*, *q90*, *q50*) are consistent with the results of Blenkinsop et al. (2015), where the scaling values for most of the gauges rise for the higher percentiles (Fig. S2 in the Supplementary material). This is also the case for the two durations of 3 h and 6 h. However, for longer durations, the scaling values vary; either rising or declining for the higher percentiles. As regards the significance of the results for different percentiles, it was found that most of the gauges show significant scaling results for rainfall volume for higher percentiles and especially for short durations. For example, all the gauges show significant results except four and eight gauges for the durations of 1-h and 3-h respectively.

An investigation of the scaling values for summer rainfall fractions revealed that the results for all the durations and for the four fractions were insignificant for the high percentile *q99* for all the stations, thus the calculation was repeated for lower percentiles (*q90, q50).* The results show that the scaling values for the last two fractions are lower for lower percentiles for most of the stations. However, for the first two fractions, the scaling values vary across the stations, either rising or falling for lower percentiles. In addition, the significance of the results increased for lower percentiles and all durations, which is opposite to the results for the scaling volume.

Apart from the significance of the results, for all percentiles and each duration, the temporal pattern shows the same structure as that described above for rainfall without seasonal separation; it peaks in the first rank fraction, which has the largest positive scaling, while the largest negative scaling appears in the fourth rank fraction. The intermediate fractions exhibit a decline in scaling by increasing rank (Fig. S3 in the Supplementary material).

4.2.2. Scaling values for winter season storms

The scaling values for rainfall volume and five durations were also analysed for the winter season (Fig. S4 in the Supplementary material). The results are interesting and completely opposite to those for the summer season. The scaling values were lowest for the shorter durations, but after the duration of 3 h (shown by most of the stations) the scaling value rose gradually by duration increase, where the largest scaling value is shown mostly for the 24-h duration. This is because stratiform storms dominant winter season storms. As in Blenkinsop et al. (2015), the scaling value for the winter hourly rainfall volume is higher for lower percentiles, which also the same for the duration of 3 h. While for longer durations most of the gauges show lower scaling values for lower percentiles. It is worth noting that the number of gauges which show significant scaling results for rainfall volume is higher for the winter season than for the summer season for all durations and all percentiles. In contrast, the number of gauges that show significant results for the scaling fractions for the winter season is lower than that for the summer season for all durations and specifically the percentile *q90*. Table S1 summarizes the number of gauges showing positive and negative scaling values for all durations, percentiles, and storms (i.e. storms with and without seasonal separation) regardless of the significance of the results.

Again, the temporal pattern for the winter season has a structure that peaks at the first rank fraction, while the lowest value is found at the fourth rank fraction and scaling values for the other two fractions are of declining values.

The scaling values for the rainfall volume and the two seasons summer and winter are consistent with the corresponding results for the scaling of storms without seasonal separation in which no trend was obvious with respect to a regional climatic control (i.e. altitude) influencing the scaling value. In addition, no trends were observed for the two seasons from a comparison of the scaling value for each segment of the temporal pattern with those segments for different durations, which is similar to the results presented in Section 4.1.

4.2.3. Uncertainty of scaling values for seasonal storms

As mentioned earlier, the scaling results for all storms (i.e. with and without seasonal separation), all durations, and different percentiles were within the 95% confidence interval. A sample of the results is shown in Fig. 6. However, for some gauges the confidence interval of the scaling values is wide, reflecting the high uncertainty in the results for those gauges. This uncertainty may have been caused by the temporal length of the gauges (i.e. 12 years) adopted for the study, or by the number of storms used to derive the scaling values (i.e. 500). Therefore we tested the effect of these two sources of uncertainty on the scaling results, as discussed below.

4.2.3.1. Uncertainty of scaling values resulted from number of storms. The scaling values for rainfall volume were tested against the number of storms used for deriving the scaling values. Thus, the largest 200 storm events were used instead of 500 in order to determine whether the number of storms affects the scaling value and the significance of the results (Wasko and Sharma, 2015). For the largest 200 storm events, all the gauges showed lower scaling values and insignificant results compared to the corresponding results for the 500 storm events for all durations, the two seasons summer and winter, and the high percentile *q99*. Therefore, the largest 200 storm events were tested again for the percentile *q90*, and the results for the summer season showed that the scaling value for the rainfall volume rose compared to the corresponding results for 500 storm events (Fig. S5 in the Supplementary material). This was the case for all the durations, except for the last one where the reverse occurred. However, for the winter season, reducing the number of storms resulted in increased scaling values for the first two durations, while the reverse occurred for the last two durations and the results for the third duration were almost equally divided between the number of gauges that showed higher and those that showed lower scaling values (Fig. S6 in the Supplementary material). In addition, the uncertainty bound for the largest 200 storm events and the two seasons, summer and winter are computed and compared with the corresponding results for the uncertainty bound for the largest 500 storm events. It is clear from Figs. 8 and S.7 that, in general, most of the gauges show small differences between the two uncertainty bounds for the two cases of storm events (i.e. 200 and 500). This is the case for all durations and the two seasons, summer and winter. However, in some cases, when there is a difference between the two bounds of uncertainty, this is due to the high range that is shown by the case of 200 storm events (e.g. Fig. S7, 1-h duration, gauges 4–10). It is worth noting that the effect of the uncertainty bound from the two cases of number of storm events on the peak flow of the sewer system has been addressed in Section 4.3.

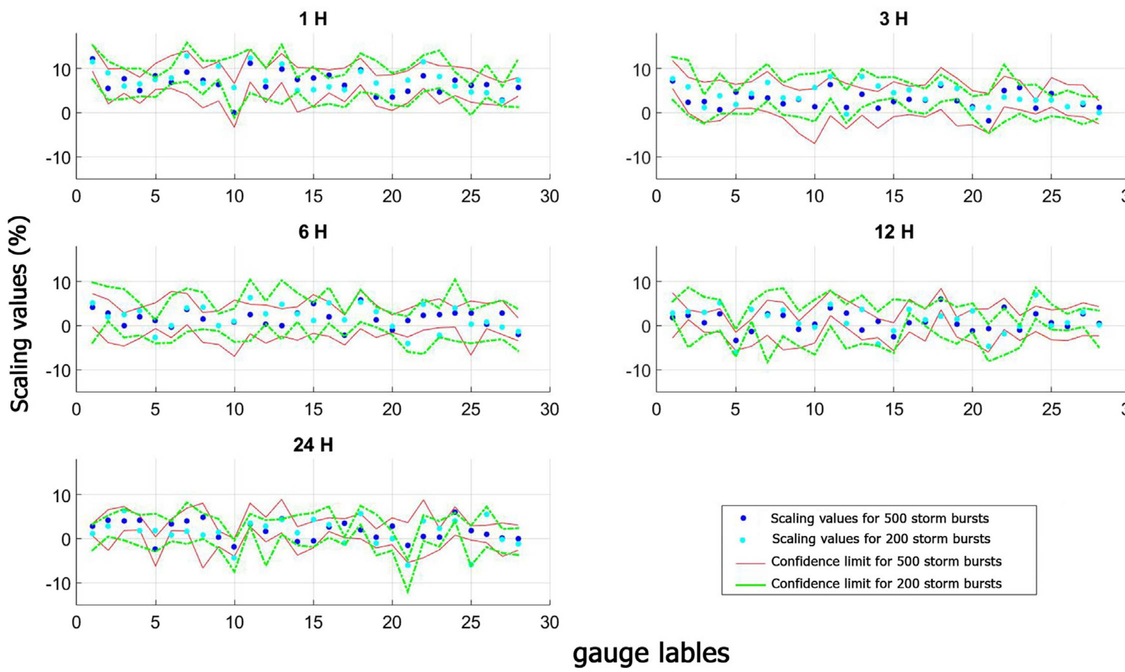

Fig. 8. Uncertainty bounds of the 95% significant level for summer rainfall scaling volume due to the effect of number of storms (i.e. largest 500 and 200 storm bursts). Each subplot is for a specific duration and the percentile *q90*.

4.2.3.2. Uncertainty of scaling values resulted from temporal length of data. The scaling values for rainfall volume were tested against the length of the data that was used to derive such values to investigate the uncertainty that may results from the temporal coverage of gauges. It is clear from the table in Fig. 1 that the gauges can be divided into three groups based on their temporal coverage, with almost one third of the total number of gauges falling into each group. Thus, the scaling values of rainfall volume for summer and winter storms calculated again based on the total length of the time series data covered by the gauges and compared to the above derived scaling volume based on the common period for all gauges, which was 12 years (2004–2015). In order to make it easier to visualise how the scaling volume can change based on the length of the data, the differences in the scaling volume based on different temporal coverage from the corresponding values based on the 12 common years are calculated and sample of the results presented in Fig. 9 for the summer storms. It is clear from Fig. 8 that the length of datasets have a considerable effect on the derived scaling values because for each duration more than one third of the total number of gauges shows higher differences in the scaling volume. The derived scaling volume based on the most recent and common period for all gauges shows higher values compared to that based on different temporal coverage. This is the case for most of the gauges which shows differences in the scaling results within the durations of 1 h, 6 h and 24 h (green circles in Fig. 9), while the reverse occurred for the durations of 3 h and 12 h (orange squares in Fig. 9). The effect of the data temporal length on the derived scaling volume for winter storms are consistent with the above results for summer storms in which there is no period that produces the highest scaling volume for all durations (Fig. S8 in the Supplementary material). It is clear from the above results that it is not essential that the most extreme rainfall values occur within the most recent period. In other words, it is not essential that the most recent period is warmer than the previous periods or that it produces the most intense and extreme rainfall events, as confirmed by Fadhel et al. (2017). Consequently, the length of data can be considered as an important source of uncertainty that may affect the scaling results. However, it should be noted that while the results of this study are based on only 12 years of data, they are still of value (especially as this study is the first of its kind conducted in the UK) and can give an indication about the future changes in rainfall extremes in the UK and how they may affect the flooding of sewer systems.

A further analysis of the effect of the length of data (i.e. gauges with different and same temporal coverage) on the scaling results for rainfall fractions revealed that the differences in the results for the gauges with different temporal coverage were much less noticeable than the corresponding differences for scaling volume.

Finally, by comparing the results of the UK and Australia, it is found that the scaling values of rainfall volume and first and last rainfall fractions for the summer season for the UK are larger than the corresponding results for Australia. This is the case when extracting storms based on the largest 500 and 200 storm events. However, the opposite behaviour is observed for the winter season storms. To explain this, previous studies show that the scaling relationship can be decomposed into thermodynamic and dynamic contributions (Emori and Brown 2005; Chen et al., 2011). Pfahl et al. (2017) show that regional differences in extreme rainfall and scaling values around the globe are mainly due to the dynamic contribution (see Fig. 3 in Pfahl et al. (2017)). The effect of this dynamic contribution is related to the change in the vertical pressure velocity, the direct radiative response to the increase of CO_2, and other factors (see Pfahl et al. (2017) for more details). This effect may therefore explain the difference between the scaling results for the UK in this study and those for Australia in Wasko and Sharma, 2015.

4.3. Impact of rainfall temporal pattern scaling on the sewer system

The peak flow magnitude of a flood is significantly affected by changes in the rainfall pattern over time (Ball, 1994; Singh and Woolhiser, 2002). Generally, a more devastating flood peak is caused by less uniform storm events that lead to a greater return interval. In this study, the effect of the temporal pattern of rainfall on the percentage relative change between the peak flow of the current climate and that of the future climate and on the number

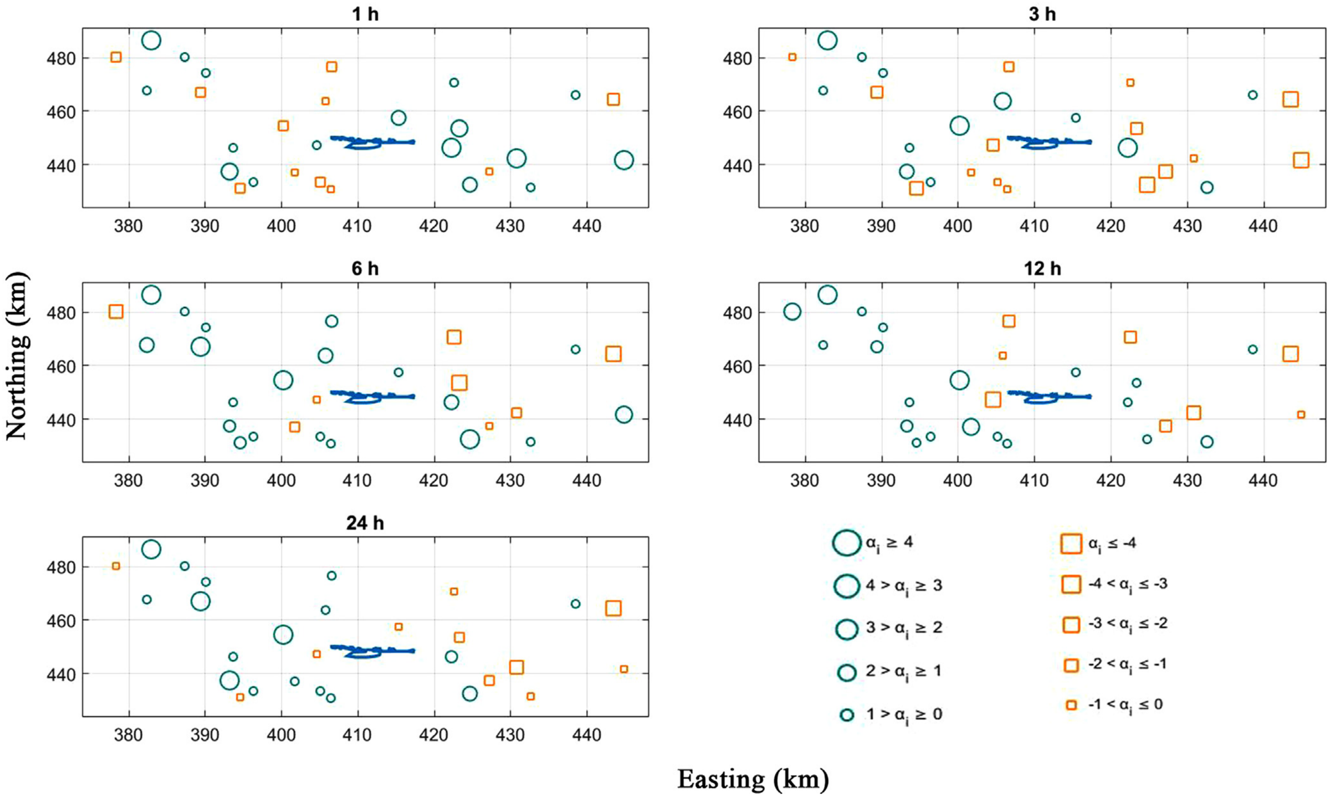

Fig. 9. Differences in scaling volume based on the length of data for the summer season and the percentile *q90*. Each subplot is for a specific duration. Green circles correspond to higher scaling values derived based on the common period, while orange squares correspond to higher scaling values derived based on different temporal coverage. (For interpretation of the references to colour in this figure legend, the reader is referred to the web version of this article.)

of flooded nodes due to the temperature rise from climate change was investigated by using the Infoworks CS model.

Previous derived design storms in the UK showed that the 50% summer profile is appropriate for urban areas, while the 75% winter profile is better for rural areas (FSR, 1975; FEH, 1999). The 50% summer profile is peakier than the 75% winter profile and, consequently, the former produces a higher peak flow and higher possibility of flooding. In addition, the scaling values for the summer season derived in Section 4.2.1 are higher than the corresponding results for the winter season in Section 4.2.2. Thus, the derived scaling and temporal pattern for the summer season were adopted for this part of the study.

The temporal patterns for 1-h and 3-h durations were built by using the average scaling results from the nearest three gauges to the study area to overcome the problems of varied scaling and the varied significant results that were shown by the nearest gauges. The rainfall values for the current and future climates for the above two durations were extracted from the IDF curves that were recently derived for the study area by Fadhel et al. (2017) and for each of the six return periods (the values of the return periods are shown in Table 1). Fadhel et al. (2017) derived eight cases of IDF curves based on eight reference periods, which were used to bias correct the modelled rainfall data in order to overcome the uncertainty that results from the constant bias assumption during the bias correction based on one reference period. Thus, for the future climate, the rainfall values for the mean and maximum climate ensemble members over the eight reference periods were used in the analysis of this study. The percentage change in the peak flow between the current and future climates as well as the number of flooded nodes were explored by adopting two different approaches.

In the first approach, it was assumed that the same current rainfall intensity would appear in the future (i.e. no scaling for the rainfall volume was applied), thus, only the temporal pattern underwent scaling using a temperature range from 1 °C to 5 °C. Also, in this approach, the rainfall intensity was disaggregated into finer time steps by applying the derived temporal pattern of each of the two structures, A and B (Fig. 5), in order to determine the extent to which the type of temporal pattern affects the change in peak flow between the current and future climate. In cases where the temporal pattern did not add to unity after scaling, it was scaled to ensure that the rainfall volume did not change across the range of temperature rises (Wasko and Sharma, 2015). In the second approach, both the rainfall volume and the rainfall fractions for the current climate were scaled with the above range of temperatures, and only the temporal pattern of structure A was applied. In cases where the rainfall volume after scaling for a temperature increase of 5 °C was less than the extracted value of the maximum climate ensemble member from the IDF curves in Fadhel et al. (2017), the temporal pattern was applied for such an extracted value. However, if the scaled rainfall volume for a specific temperature was higher than the maximum climate ensemble member, then the rainfall volume for that temperature and the other higher temperature values were not taken into account in the analysis.

For the two approaches, the six return periods for the extracted rainfall intensities from the IDF curves were assumed to be the same as the return periods for the peak flow (Butler and Davies 2011; Willems, 2013). Table 1 shows an example of the percentage increase in peak flow for the flow monitor FM015; the two approached of rainfall temporal scaling; six return periods; and the duration of 1 h. While Table 2 shows sample of the results of

the percentage increase in peak flow for four flow monitors; the two approached of rainfall temporal scaling; the return period of 2 years; and the two durations 1 h and 3 h.

4.3.1. Impact of rainfall temporal pattern scaling on sewer peak flow

As a result of scaling only the temporal pattern, the derived pattern of type A and flow monitor FM015 shows that for a 1-h rainfall duration and each return period, the percentage of peak flow keeps increasing as the temperature rises (Table 1). However, for a specific temperature value there was no particular trend for the percentage increase in peak flow as the return period increases. For example, increasing the temperature from 1 °C to 5 °C results in the highest percentage increase in peak flow for the 2-year return period, where the peak flow rises from 1.31% per 1 °C to 6.28% per 5 °C. On the other hand, the lowest percentage increase occurs in the case of two return periods, 50 years (for the temperature values 2 °C and 4 °C) and 100 years (for the temperature values 1 °C, 3 °C, and 5 °C), where the peak flow rises from 0.44% per 1 °C to 3.68% per 5 °C.

From a comparison of the above results with those for the derived temporal pattern of type B, it is clear that the pattern of type A produces a higher percentage increase in peak flow than that of type B for the last three return periods and the temperature rise from 1 °C to 5 °C (Table 1). On the other hand, type B shows the largest values for the percentage change in peak flow between the current and future climates for the second return period. The highest percentage of peak flow for the first and third return periods varies between the two types of temporal pattern for a range of temperature rises. However, as regards the difference in the magnitude of the percentage increase in peak flow between the two temporal patterns, it is clear from the table that in some cases the two patterns show close results but with some differences (e.g. the first return period), while in other cases the difference is high, at almost double (e.g. the last three return periods and especially the last three temperature values). In addition, Fig. S9 shows the flow-duration-frequency (FDF) graph for flow monitor FM015 produced by scaling only the temporal pattern for the temperature range 1 °C to 5 °C, six return periods, and the two temporal patterns of structures A and B.

The sensitivity of the relative change in peak flow to future temperature change was also tested by scaling both the rainfall volume and the rainfall fractions (by applying the temporal pattern of type A) for a temperature rise from 1 °C to 5 °C. The results for flow monitor FM015 show that the change in peak flow between the current and future climates for a 1-h rainfall duration after scaling the rainfall volume and fractions is much greater than the corresponding results produced by scaling the temporal pattern alone (Table 1). For example, for a 5-year return period the peak flow increases from 10.85% per 1 °C to 60.50% per 5 °C compared to 1.13% per 1 °C to 5.79% per 5 °C by scaling only the temporal pattern of type A. It is worth noting that when scaling rainfall volume and fractions the percentage increase in the peak flow declines as the return period increases for a specific temperature. However, it increases as the temperature rises for a specific return period.

The above analysis was repeated for the 3-h duration and all six return periods. For this duration and for flow monitor FM015, by scaling the temporal pattern only, the pattern of type B shows a higher percentage increase in the peak flow between the current and future climates than type A for all six return periods (the results not shown). On the other hand, scaling both the rainfall volume and the rainfall fractions produces a change in the peak flow for the 3-h duration that is similar to that for the 1-h duration, i.e. the percentage increase in the peak flow is higher than when scaling only the rainfall fractions. However, the percentage change in the peak flow between the current and future climates for the 3-h duration and flow monitor FM015 are much lower than the corresponding results for the 1-h duration (Table 2 for FM015). In addition, for a specific temperature, applying both of the approaches to scaling to the 3-h duration leads to almost constant results for the percentage change in the peak flow over the return periods. For example, by scaling both the rainfall volume and fractions for a 5 °C increase in temperature, the percentage of increase for peak flow was around 21% for the six return periods. It is worth noting that for the 3-h duration and each return period, none of the scaled rainfall volumes for the temperature rise of 5 °C are close to those of the corresponding rainfall intensity of the maximum climate ensemble member. Thus, the temporal pattern applied for the future rainfall intensity and each return period, and the results for the percentage change in peak flow shown in Table 2 are the highest values over the temperature range for each return period. In addition, the FDF graph for flow monitor FM015 by scaling both rainfall volume and rainfall fractions is shown in Fig. S10 for the temperature range 1 °C to 5 °C, six return periods, and the temporal pattern of structure A.

The above analysis of flow monitor FM015 was repeated for the other 15 flow monitors and Table 2 shows sample of the results for four flow monitors. The results for most of the flow monitors are consistent, where for each return period the size of the peak flow for the future climate increases as the temporal pattern of the rainfall changes due to the rise in temperature. The percentage increase is higher when both the rainfall volume and the temporal pattern are scaled. However, no obvious trend was observed by all flow monitors regarding the maximum increase in the percentage change of peak flow with the return periods for a specific rise in temperature. When only the temporal pattern is scaled, the results for the two types of patterns with different structures show that for each duration neither pattern can produce the maximum percentage increase in peak flow for all temperature ranges; all return periods; and all flow monitors. It is worth noting that for some flow monitors, the percentage change in the peak flow between the

Table 1
Percentage of change of peak flow between the current and future climates for flow monitor FM015 and the duration of 1 h due to the increase in temperature.

Temp Range °C	Scaling rainfall fractions only												Scaling rainfall volume and rainfall fractions					
	Temporal pattern of type B						Temporal pattern of type A						Temporal pattern of type A					
	2 year	5 year	10 year	25 year	50 year	100 year	2 year	5 year	10 year	25 year	50 year	100 year	2 year	5 year	10 year	25 year	50 year	100 year
1	1.29	1.93	2.60	0.58	0.20	0.44	1.31	1.13	1.25	1.04	0.85	0.44	12.57	10.85	10.39	8.99	7.72	6.95
2	2.13	3.98	3.30	1.47	1.00	1.10	2.49	2.25	2.28	1.93	1.30	2.04	25.72	21.86	21.35	17.45	15.43	13.92
3	3.98	4.99	3.45	1.48	1.07	1.40	3.79	3.08	3.73	3.44	2.86	2.63	39.34	35.47	31.80	26.55	22.51	20.45
4	4.82	5.53	4.42	2.16	2.22	1.97	4.86	4.71	4.35	3.44	3.17	3.28	54.04	48.41	41.93	34.53	29.27	28.91
5	5.63	6.81	4.79	3.46	2.80	2.08	6.28	5.79	5.48	4.28	4.11	3.68	–	60.50	51.17	41.93	38.32	38.31
															61.10	**51.22**	**48.36**	**43.27**

Bold numbers mean the temporal pattern applied for rainfall value of the maximum climate ensemble member extracted from IDF curves, while '–' mean the scaled rainfall value at that temperature exceed the rainfall value of the maximum climate ensemble member extracted from IDF curves.

Table 2
Percentage of change of peak flow between the current and future climates for return period of 2 years due to the increase in temperature.

Duration	Temp Range °C	Scaling rainfall fractions only								Scaling rainfall volume and fractions			
		Temporal pattern of type B				Temporal pattern of type A				Temporal pattern of type A			
		FM001	FM015	FM018	FM115	FM001	FM015	FM018	FM115	FM001	FM015	FM018	FM115
1 h	1	0.48	1.29	0.65	1.16	0.69	1.31	0.51	0.55	6.13	12.57	6.67	4.73
	2	0.78	2.13	1.23	1.46	1.35	2.49	1.08	1.27	10.00	25.72	15.12	8.23
	3	1.1	3.98	1.52	1.71	1.99	3.79	1.73	1.75	13.21	39.34	24.18	13.38
	4	1.38	4.82	2.13	2.24	2.59	4.86	2.30	2.35	15.77	54.04	33.75	19.53
	5	1.71	5.63	2.69	2.66	3.28	6.28	2.76	2.71	–	–	–	–
3 h	1	1.35	1.32	0.55	1.24	1.21	1.16	0.48	1.11	5.26	5.13	2.11	4.80
	2	2.66	2.6	1.08	2.44	2.40	2.31	0.96	2.19	10.63	10.47	4.21	9.82
	3	3.95	3.85	1.59	3.62	3.55	3.43	1.41	3.25	16.29	16.05	6.49	15.09
	4	5.21	5.07	2.09	4.77	4.67	4.53	1.86	4.28	21.76	21.86	8.86	20.60
	5	6.43	6.27	2.57	5.89	5.76	5.60	2.29	5.28	28.41	27.93	11.25	26.39
										57.11	**58.87**	**23.62**	**56.34**

Bold numbers mean the temporal pattern applied for rainfall value of the maximum climate ensemble member extracted from IDF curves, while '–' mean the scaled rainfall value at that temperature exceed the rainfall value of the maximum climate ensemble member extracted from IDF curves.

current and future climates is much higher than for others, and this seems to depend on the sub-catchment area that drains to the flow monitor.

Finally the uncertainty range for the percentage of peak flow was checked by scaling both the rainfall volume and rainfall fraction for all flow monitors. For this analysis we only adopt the temporal pattern of structure A and the temperature range 1 °C to 5 °C and for the two cases of storm numbers (i.e. largest 500 & 200 storm events). Fig. S11 shows the sample of the results for the flow monitor FM015 and 1-h duration. It is clear from the figure that for each return period the uncertainty bound for the percentage change of peak flow increases for higher temperatures. Also, when comparing the uncertainty bound for all return periods and a specific temperature, such uncertainty increases for longer return periods. This is the case when testing the uncertainty bound for both the largest 500 & 200 storm events. In addition, there is a small difference between the two uncertainty bounds for the two cases of storm numbers.

4.3.2. Impact of rainfall temporal pattern scaling on flooded nodes

As a result of scaling the rainfall fractions on the number of flooded nodes, the two derived patterns A and B show almost the same results for the number of flooded nodes for each return period over the range of temperature increases. Table 3 shows the sample of the results of the flooded nodes for the two approached of rainfall temporal scaling; six return periods; and the duration of 1 h. For the two durations of 1 h and 3 h, the number of flooded nodes increases as the return period increases. However, the occurrence of dangerous flooding is not indicated by the two temporal patterns for the first two return periods and for the whole range of temperature increases. In addition, for the two durations and a specific return period, as the temperature increases, the number of flooded nodes increases (e.g. return period of 10 years and pattern of type A; Table 3). For other return periods, the number of flooded nodes remains constant either for the whole or part of the range of temperature increases (e.g. return periods of 50 and 100 years and pattern of type B; Table 3). However, the largest number of flooded nodes is seen for the largest return period and a 1-h duration with a range of 30 to33 nodes flooded over the temperature increase.

The number of flooded nodes by scaling both the rainfall volume and rainfall fractions for the temporal pattern of type A are higher than the corresponding results by scaling the rainfall fractions alone (Table 3). However the results are similar to that by scaling the rainfall fractions alone, where the number of flooded nodes increases with a rise in temperature for a specific return period or with an increase in the return period for a specific temperature (Table 3). In addition, the largest number of flooded nodes occurs for the 1-h duration, compared to the results for the 3-h duration, and especially for the last return period (100 years) where the flooded nodes increase from 38 nodes for a 1 °C increase to 63 nodes for a 5 °C increase in temperature.

The uncertainty bound for the number of flooded nodes was checked by scaling the rainfall volume and rainfall fractions for the temporal pattern of type A. The results are shown in Fig. S12 and for the two cases of the number of storms (i.e. largest 500 & 200 storm events). The uncertainty bounds in Fig. S12 increases as the temperature rises for a specific return and as the return period increases for a specific temperature. This is the case for the largest 500 & 200 storm events. In addition, the uncertainty bound for the two cases of the number of storms shows only a small difference.

Table 3
Number of flooded nodes for 1 h duration due to climate change.

	Scaling rainfall fractions only												Scaling rainfall volume and rainfall fractions					
	Temporal pattern of type B						Temporal pattern of type A						Temporal pattern of type A					
Temp Range °C	2 year	5 year	10 year	25 year	50 year	100 year	2 year	5 year	10 year	25 year	50 year	100 year	2 year	5 year	10 year	25 year	50 year	100 year
0	0	2	7	19	25	30	0	0	6	17	24	30	0	0	6	17	24	30
1	0	2	8	19	25	30	0	1	7	19	24	30	0	5	16	22	30	38
2	0	2	8	21	25	30	0	1	7	19	24	32	0	8	19	28	38	42
3	0	2	8	21	25	31	0	1	8	19	24	33	0	16	24	38	43	54
4	0	2	9	21	25	31	0	1	9	19	25	33	3	19	30	42	54	58
5	0	3	10	22	25	33	0	1	9	20	25	33	5	25	38	54	58	63

Zero temperature value mean current climate.

5. Conclusions

Due to the lack of long-term flow data, design storms are still widely used in engineering practice to simulate design floods in sewer systems and to analyse the flood risk. One of the drawbacks of such storms is the fixing of the shape of the temporal profile of rainfall. However, previous studies showed that due to climate change each fraction of the rainfall profile scales with temperature in a different way. In other words, peak fractions become peakier and non-peak fractions become less so with the temperature rise due to climate change. Consequently, such changes in the storm profile may affect the peak flow of the drainage system and produce flooding. Thus, the sensitivity of peak flow to the changes in the temporal pattern of rainfall has been investigated by examining the scaling relationship between rainfall and temperature using the nearest 28 gauges to the study area.

The scaling values for the rainfall volume and the rainfall fractions were calculated with and without seasonal separation. It was found that the scaling results for rainfall volume without seasonal separation were very different from the corresponding results for rainfall volume with seasonal separation for all durations. Specifically, the largest scaling values were seen for hourly summer storms, and such values declined as the duration increased up to a certain limit (12 h) and then scaling increased again for the last duration; however, this value was still lower than those for shorter durations. The opposite behaviour was observed for the winter season, where the scaling values were found to be the lowest for short durations (1h, 3 h) and got bigger with increasing duration, where the largest value was mostly commensurate with the longest duration (24 h). For all the data with and without seasonal separation, there was no trend for the regional climatic controls on the scaling value.

From an examination of the scaling values of temporal patterns within individual storm events, it was found that there was a consistent positive scaling for the largest rainfall fraction and a consistent negative scaling for the smallest rainfall fraction. This was the case for storms with and without seasonal separation, but there were also clear differences in the fraction scaling values between storm types. In addition, it was observed that the results for fraction scaling were insignificant for the high percentile *q99.* This was the case for the last two durations and storms without seasonal separation, and for all durations for seasonally separated storms. As for lower percentiles (*q90, q50*), the number of stations that showed significant results increased for all durations, all fractions, and storms for the two seasons summer and winter.

The derived temporal pattern for the summer season was applied to a hydrodynamic sewer model in order to study the sensitivity of the peak flow to changes in the rainfall pattern due to climate change. To this end, two different approaches were adopted. First, the rainfall volume was fixed and the temporal pattern alone was scaled by applying and comparing two of the derived patterns for the summer season. Second, both the rainfall volume and the rainfall fractions were scaled with temperature change for only one pattern. The percentage increase in the peak flow of 16 flow monitors as a result of scaling both the rainfall volume and fractions was found to be much greater than the corresponding results caused by scaling only the temporal pattern. This was the case for the two durations (1h, 3 h); all return periods; and all temperature values. However, there was no specific temporal pattern that could show the maximum growth in the change of future peak flow for all return periods and the two durations when scaling the temporal pattern alone.

In addition, the number of flooded nodes by scaling both the rainfall volume and the rainfall fractions were higher than the corresponding results by scaling the rainfall fractions alone. The largest number of flooded nodes were shown for the shorter durations, larger return periods, and the highest increase of temperature.

Changes in peak flow due to climate change may result in serious consequences for sewer systems and thus this aspect should be considered in the decision-making process for designing new systems or upgrading the existing systems. The worst case scenario should be addressed carefully; even though it may not be used in the actual sewer system design, it can still give an indication as to how to mitigate sewer flooding through the adoption of flexible and sustainable solutions (Willems et al., 2012; Willems, 2013; Fadhel et al., 2017).

Further research is required to examine some as yet untackled questions. For example, what results will be produced if the scaling values for the rainfall fractions are derived from another network with finer resolution? (so the temporal pattern can be divided into more than four fractions). By classifying the rainfall into convective and stratiform storms, does the scaling results be similar to the corresponding results of storms based on seasonal separation? Also, how will those results affect the peak flow and how the uncertainty of peak flow will be compared with the uncertainty of scaling volume? Even more interestingly, how will the results vary for different study areas? It is hoped that this study will stimulate the community to explore such questions further.

Acknowledgments

The authors thank the Environment Agency (https://www.gov.uk/government/organisations/environment-agency), for providing the rain gauges dataset. We also thank the Centre of Ecology and Hydrology for providing the gridded temperature data through (CHESS-met) dataset. More details about the CHESS-met data are available from https://catalogue.ceh.ac.uk/documents/b745e7b1-626c-4ccc-ac27-56582e77b900. The authors would like to thank Yorkshire Water Service Ltd. for providing the rainfall data for the urban catchment, as well as the sewer flow data and Infoworks CS model of the sewer system.

Appendix A. Supplementary data

Supplementary data associated with this article can be found, in the online version, at https://doi.org/10.1016/j.jhydrol.2018.03.041.

References

Ball, J.E., 1994. The influence of storm temporal patterns on catchment response. J. Hydrol. 158, 285–303. https://doi.org/10.1016/0022-1694(94)90058-2.

Berg, P., Haerter, J.O., Thejll, P., Piani, C., Hagemann, S., Christensen, J.H., 2009. Seasonal characteristics of the relationship between daily precipitation intensity and surface temperature. J. Geophys. Res.-Atmospheres 114. Artn D18102 10.1029/2009jd012008.

Berg, P., Haerter, J.O., 2011. Unexpected increase in precipitation intensity with temperature – a result of mixing of precipitation types? Res. Atmos. https://doi.org/10.1016/j.atmosres.2011.05.012.

Berg, P., Moseley, C., Haerter, J.O., 2013. Strong increase in convective precipitation in response to higher temperatures. NatureGeosci. 6, 181–185. https://doi.org/10.1038/ngeo1731.

Blenkinsop, S., Chan, S.C., Kendon, E.J., Roberts, N.M., Fowler, H.J., 2015. Temperature influences on intense UK hourly precipitation and dependency on large-scale circulation. Environ. Res. Lett. 10 (5). Artn 05402110.1088/1748-9326/10/5/054021.

Butler, D., Davies. J.w., 2011. Urban Drainage. Spon Press, Taylor & Francis, p. 625p.

Centre for Ecology & Hydrology, 1999. The Flood Estimation Handbook (five volumes). Volume 3: Statistical procedures for flood frequency estimation. Wallingford, UK.

Chan, S.C., Kendon, E.J., Roberts, N.M., Fowler, H.J., Blenkinsop, S., 2016. Downturn in scaling of UK extreme rainfall with temperature for future hottest days. Nat. Geosci. 9, 24–28. https://doi.org/10.1038/ngeo2596.

Chen, G., Ming, Y., Singer, N.D., Lu, J., 2011. Testing the Clausius-Clapeyron constraint on the aerosol-induced changes in mean and extreme

precipitation. Geophys. Res. Lett. 38, L04807. https://doi.org/10.1029/2010GL046435.

Desbordes, M., 1978. Urban runoff and design storm modelling. In: Proc. of the First International Conference on Urban Storm Drainage. U.K. Pentech Press, London, U.K., pp. 353–361.

Emori, S., Brown, S.J., 2005. Dynamic and thermodynamic changes in mean and extreme precipitation under changed climate. Geophys. Res. Lett. 32, L17706. https://doi.org/10.1029/2005GL023272.

Fadhel, S., Rico-Ramirez, M.A., Han, D., 2016. Exploration of an adaptive merging scheme for optimal. J. Hydroinformatics. https://doi.org/10.2166/hydro.2016.022.

Fadhel, S., Rico-Ramirez, M.A., Han, D., 2017. Uncertainty of Intensity-Duration-Frequency (IDF) curves due to varied climate baseline periods. J. Hydrol. 547, 600–612. https://doi.org/10.1016/j.jhydrol.2017.02.013.

Hardwick Jones, R., Westra, S., Sharma, A., 2010. Observed relationships between extreme sub-daily precipitation, surface temperature, and relative humidity. Geophys. Res. Lett. 37, L22805. https://doi.org/10.1029/2010GL045081.

Huff, F.A., 1967. Time distribution of rainfall in heavy storms. Water Resour. Res. 3 (4), 1007–1019. https://doi.org/10.1029/WR003i004p01007.

Intergovernmental Panel on Climate Change (IPCC), 2012. Managing the risks of extreme events and disasters to advance climate change adaptation. In: Field, C. B., et al. (Eds.) A Special Report of Working Groups I and II of the Intergovernmental Panel on ClimatChange, Cambridge University Press, New York.

James, W., Robinson, M., 1982. Continuous Models Essential for Detention Design. In: Proceedings, Stormwater Detention Facilities. ASCE, Henniker, New Hampshire, pp. 163–175.

Jones, M.R., Blenkinsop, S., Fowler, H.J., Kilsby, C.G., 2014. Objective classification of extreme rainfall regions for the UK and updated estimates of trends in regional extreme rainfall. Int. J. Climatol. 34, 751–765. https://doi.org/10.1002/joc.3720.

Kiefer, C.J., Chu, H.H., 1957. Synthetic storm pattern for drainage design. J. Hydraul. Div., Proc. Am. Soc. Civil Eng. 83 (13). 32-1-13 3 2-25.

Koenker, R., 2005. Quantile Regression. Cambridge U. Press.

Koenker, R. 2013, quantreg: Quantile Regression. [Available at http://CRAN.R-project.org/package5quantreg.]

Lenderink, G., van Meijgaard, E., 2008. Increase in hourly precipitation extremes beyond expectations from temperature changes. Nat. Geosci. 1 (8), 511–514. https://doi.org/10.1038/ngeo262.

Lenderink, G., Mok, H.Y., Lee, T.C., van Oldenborgh, G.J., 2011. Scaling and trends of hourly precipitation extremes in two different climate zones: Hong Kong and the Netherlands. Hydrol. Earth Syst. Sci. 15 (9), 3033–3041. https://doi.org/10.5194/hess-15-3033-2011.

Liguori, S., Rico-Ramirez, M.A., Schellart, A.N.A., Saul, A.J., 2012. Using probabilistic radar rainfall nowcasts and NWP forecasts for flow prediction in urban catchments. Atmos. Res. 103, 80–95. https://doi.org/10.1016/j.atmosres.2011.05.004.

Madsen, H., Mikkelsen, P.S., Rosbjerg, D., Harremoes, P., 2002. Regional estimation of rainfall intensity-duration-frequency curves using generalized least squares regression of partial duration series statistics. Water Resour. Res. 38 (11). Artn 1239 10.1029/2001wr001125.

McPherson, M.B., 1978. Urban Runoff Control Planning EPA-600/9-78-035. Environmental Protection Agency, Washington, DC.

Müller, T.M., SchützeBárdossy, A., 2017. Temporal asymmetry in precipitation time series and its influence on flow simulations in combined sewer systems. Adv. Water Res. 107, 56–64. https://doi.org/10.1016/j.advwatres.2017.06.010.

NERC 1975. Flood Studies Report (five volumes). Natural Environment Research Council London (Vol. II, Meteorological Studies)

Nguyen, V.-T.-V., Desramaut, N., Nguyen, T.D., 2010. Optimal rainfall temporal patterns for urban drainage design in the context of climate change. Water Sci. Technol. 62 (5), 1170–1176. https://doi.org/10.2166/wst.2010.295.

Packman, J., 1990. New Hydrology model. WaPUG Spring Meeting. http://www.ciwem.org/groups/wapug/ Accessed May 2011.

Pfahl, S., O'Gorman, P.A., Fischer, E.M., 2017. Understanding the regional pattern of projected future changes in extreme precipitation. Nat. Clim. Change 7. https://doi.org/10.1038/NCLIMATE3287.

Pilgrim, D.H., Cordery, I., 1975. Rainfall temporal patterns for design floods. J. Hydraulics Division-Asce 101 (Nhy1), 81–95.

Rico-Ramirez, M.A., Liguori, S., Schellart, A.N.A., 2015. Quantifying radar-rainfall uncertainties in urban drainage flow modelling. J. Hydrol. 528, 17–28. https://doi.org/10.1016/j.jhydrol.2015.05.057.

Rivard, G., 1996. Design storm events for urban drainage based on historical rainfall data: a conceptual framework for a logical approach. J. Water Manage. Model. Rl91-12. doi: 10.14796/JWMM.Rl91-12.

Robinson, E.L., Blyth, E., Clark, D.B., Finch, J., Rudd, A.C., 2015. Climate hydrology and ecology research support system potential evapotranspiration dataset for Great Britain (1961–2012) [CHESS-PE]. NERC Environ. Inf. Data Centre. https://doi.org/10.5285/d329f4d6-95ba-4134-b77a-a377e0755653.

Sarginson, E.J., & Nussey, B.B., 1982. The explicit computation of urban runoff. Urban Drainage Systems: Proceedings of the First International Seminar, Southampton, England. September 1982 ISBN 0273085964.

Sifalda, V., 1973. Entwicklung eines Berechnungsregens fur diё Bemessung von Kanalnetzen. GWF-Wasser/Abwasser 114, 435–440.

Singh, V.P., Woolhiser, D., a., 2002. Mathematical modeling of watershed hydrology. J. Hydrol. Eng. 7, 270–292. https://doi.org/10.1061/(ASCE)1084-0699(2002) 7:4(270).

Walesh, S.G., 1979. Summary Seminar on the Design Storm Concept. Proceedings, Stormwater Management Model (SWMM) Users Group meeting, EPA 600/9-79-026.

WaPUG, 2002. Code of practice for the hydraulic modelling of sewer systems Accessed May 2011 http://www.ciwem.org/groups/wapug/, .

Wasko, C., Sharma, A., 2014. Quantile regression for investigating scaling of extreme precipitation with temperature. Water Resour. Res. 50 (4), 3608–3614. https://doi.org/10.1002/ 2013WR015194.

Wasko, C., Sharma, A., 2015. Steeper temporal distribution of rain intensity at higher temperatures within Australian storms. Nat. Geosci. 8 (7). https://doi.org/10.1038/Ngeo2456. 527-U166.

Wenzel H. G. 1982. Rainfall for urban stormwater design. In: Urban Storm Water Hydrology. Water Resour. Mongor. Ser., 7, D.F. Kibler (ed.), American Geophysical Union, Washington, DC, pp. 35-67.

Willems, P., 2000. Compound intensity/duration/frequency-relationships of extreme precipitation for two seasons and two storm types. J. Hydrol. 233, 189–205. https://doi.org/10.1016/S0022-1694(00)00233-X.

Willems, P., 2013. Revision of urban drainage design rules after assessment of climate change impacts on precipitation extremes at Uccle, Belgium. J. Hydrol. 496, 166–177. https://doi.org/10.1016/j.jhydrol.2013.05.037.

Willems, P., Olsson, J., Arnbjerg-Nielsen, K., Beecham, S., Pathirana, A., Gregersen, I. B., Madsen, H., Nguyen, V.T.V., 2012. Impacts of Climate Change on Rainfall Extremes and Urban Drainage Systems. IWA Publishing, London.

Yen, B.C., Chow, V.T., 1980. Design hyetographs for small drainage structures. J. Hyd. Div., Am. Soc Civil Eng. 106 (HY6), 1055–1076.